ISSN 1027-4510, Journal of Surface Investigation. X-ray, Synchrotron and Neutron Techniques, 2015, Vol. 9, No. 4, pp. 765–770. © Pleiades Publishing, Ltd., 2015.
Original Russian Text © M.V. Zorina, I.M. Nefedov, A.E. Pestov, N.N. Salashchenko, S.A. Churin, N.I. Chkhalo, 2015, published in Poverkhnost'. Rentgenovskie, Sinkhrotronnye i Neitronnye Issledovaniya, 2015, No. 8, pp. 9–15.

Precision Aspherization of the Surface of Optical Elements by Ion-Beam Etching

M. V. Zorina[a], I. M. Nefedov[a, b], A. E. Pestov[a, b], N. N. Salashchenko[a], S. A. Churin[a, b], and N. I. Chkhalo[a]

[a] *Institute for Physics of Microstructures, Russian Academy of Sciences, Nizhny Novgorod, 603950 Russia*
[b] *Lobachevsky State University of Nizhny Novgorod, pr. Gagarina 23, Nizhny Novgorod, 603950 Russia*
e-mail: aepestov@ipm.sci-nnov.ru

Received August 5, 2014

Abstract—Ion-beam methods are developed for forming supersmooth aspherical optical surfaces of polished fused quartz with a precision on the level of 3 nm relative to the standard deviation and 0.2–0.3 nm for the mean-square surface roughness in the range of spatial frequencies of 0.01–100 μm^{-1}.

Keywords: ion etching, shape correction, aspherization, imaging X-ray optics
DOI: 10.1134/S1027451015040394

INTRODUCTION

Aspherization of the surface of optical elements compensates geometric aberrations and expands the field of view of an optical system. One aspherical surface in a lens can replace two or three spherical surfaces, which can dramatically decrease the number of components in the system. This is particularly crucial for the soft X-ray (SXR) and extreme ultraviolet (EUV, wavelengths of 1–60 nm) ranges, since an increase in the number of reflecting surfaces reduces the total transmittance of the optical system (the reflection coefficient of one mirror is markedly different from unity). In addition, the use of short wavelengths imposes strict requirements on the accuracy of the shape (the root-mean square (RMS) deviation ~1 nm) and roughness ($\sigma \sim 0.2$–0.3 nm) of the surface. The use of aspherical surfaces significantly enhances the potential of optical systems; however, their application is limited by the complexity of their manufacture and control, since a conventional technique for manufacturing spherical surfaces based on the bedding of a workpiece and a tool cannot be used because of the variable radius of curvature of the detail. Using polishing pads with different radii of curvature often leads to the development of surface roughness in the region of middle spatial frequencies (10^{-2} to 10^{0} μm^{-1}), which is unacceptable in diffraction-quality optical systems.

The complexity of manufacturing X-ray optical elements and a lack of reliable methods for controlling their shape and surface roughness hinder the development of diffraction-quality imaging X-ray optics. Procedures developed at the Institute of Physics of Microstructures to control the form [1] and roughness over the entire range of spatial frequencies, which are responsible for formation of the image and reflection [2], made it possible to apply the method of ion-beam correction [3] in the formation of complex aspherical elements.

ION-BEAM ETCHING STAND

The study is carried out using an ion-beam etching stand [4]. The instrument is equipped with accelerated-ion sources: KLAN-103M with a filament cathode (Platar, Russia); a cold cathode source (a source with a focused ion beam; Ferri Vatt, Russia), and KLAN-163M (high-frequency plasma source, Platar, Russia). This enables operation over a wide range of energies from 50 to 1500 eV and the application of various types of gases both inert and reactive compounds, including those containing fluorine.

When working with dielectric materials, an additional thermocathode-neutralizer is used, installed at the output of the ion source which ensures full compensation of the ion-beam charge; that is, etching is conducted by means of neutral atoms.

Sources of the KLAN type generate a quasi-parallel beam of accelerated ions with apertures of ∅150 mm (KLAN-163M) and 90 × 60 mm (KLAN-103M); and the Ferri Vatt-source, using replaceable diaphragms, produces an ion beam 2 mm in diameter. The device is equipped with a five-axis goniometer, which enables the detail to be turned at a proper angle to the ion beam.

The goniometer ensures etching in the entire range of angles of ion incidence onto the sample surface; in particular, it provides a local normal to any point on a

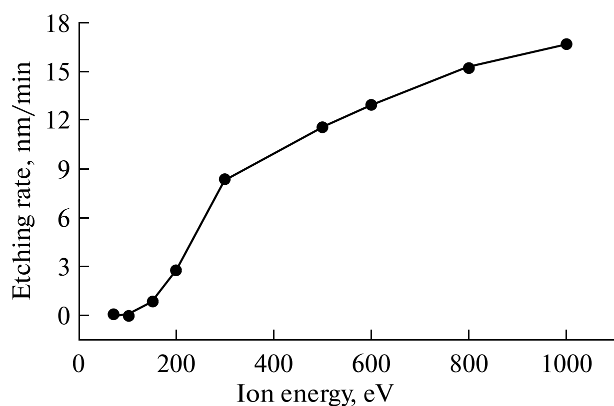

Fig. 1. Rate of SiO_2 etching depending on the energy of argon ions; $\theta_{inc} = 90°$, $j = 0.3$ mA/cm^2.

surface of any shape at the point of incidence of the ion beam and offers ion-beam scanning across the sample surface (the software specifies the coordinate matrix and exposure time at the point).

CONTROLLING SURFACE ROUGHNESS

The surface roughness is conditionally divided into two ranges: middle-frequency roughness and high-frequency roughness. The middle spatial frequency-roughness (MSFR, 10^{-2} to 1 μm^{-1}) leads to the scattering of radiation at small angles in such a way that the radiation remains in the image, but its contrast decreases, and this reduces the resolution of imaging optics. High spatial-frequency roughness (HSFR) with spatial frequencies from 1 to 10^2 μm^{-1} is a structure at which the incident radiation is scattered at large angles, leading to a decrease in the reflectance of mirrors and, as a consequence, to a decrease in the transmittance of the optical system as a whole. To ensure the calculated resolution of the imaging scheme and the quality of multilayer reflective coatings at SXR and EUV wavelengths, the effective surface roughness over the entire range of spatial frequencies should be on the level of 0.2–0.4 nm [5].

As part of the work, we studied the behavior of the surface roughness after appreciable material removal (1 μm or more) both at middle (10^{-2} to 10^0 μm^{-1}) and high (10^0 to 10^2 μm^{-1}) spatial frequencies. Polished plates of fused quartz (sort QV), subjected to deep grinding and polishing, were used as the objects of study. QV quartz is a typical substrate material of optical elements for the SXR and EUV wavelength range.

The etch depth was measured by a profiler, the surface of which was covered by a mask. As a result of etching, a step was formed on the profiler surface; the height of the step was measured using a Talysurf CCI 2000 interference microscope. The mean-square roughness of the surface was measured by atomic force microscopy (AFM) using an NT-MDT Solver P47-PRO microscope (frame size, 2×2 to 50×50 μm^2) and diffuse soft X-ray scattering with a wavelength of 13.5 nm using a laboratory reflectometer [6]. According to the results of measurements, the power spectral density (PSD) functions were plotted in the range of spatial frequencies of 0.01–100 μm^{-1}, which gave the possibility to analyze the effect of etching processes on the properties of surfaces at middle and high spatial frequencies. The PSD function is the power spectral density function of roughness, and the integral under its curve is the effective surface roughness in an appropriate range of spatial frequencies [7].

The study was carried out for an ion energy of approximately 1 keV, firstly, by virtue of a markedly higher sputtering rate, which is important when units or tens of micrometers of material is removed. Secondly, as can be seen from the graph (Fig. 1), the etching rate varies only slightly for energies from 600 to 1000 eV, which is convenient in terms of controlling the process. This means that a slight change in the etching parameters during the process does not lead to significant errors in the amount of material being removed.

Studies have shown that upon the removal of more than 1 μm of material from samples of polished fused QV quartz, subjected to the standard procedure of deep grinding and polishing and having an initial surface roughness on the level of $\sigma_{eff} = 0.25$ nm in the range of spatial frequencies of 10^{-2} to 10^2 μm^{-1}, the roughness in the middle spatial-frequency range of 10^{-2} to 10^0 μm^{-1} is retained, and in the high spatial-frequency range of 10^0 to 10^2 μm^{-1}, the surface is somewhat smoothed (Fig. 2).

The graphs shown in Fig. 2 demonstrate the roughness dynamics upon surface treatment by neutralized argon ions with an energy of 800 eV; the etching depth is 1 μm. With an increase in material removal, no further change occurs.

Thus, it was shown that ion-beam etching using argon ions with an energy of 1 keV preserves the surface roughness at an atomically smooth level and ensures deep surface asphherization of elements that are then applied in diffraction-quality optical systems.

PROCEDURE FOR SURFACE ASPHERIZATION (AXISYMMETRIC PROFILE)

Deep aspherization is a deviation from the nearest sphere by more than 30 μm. In the case of an axially symmetric profile of deviation from the nearest sphere, deep aspherization is performed using KLAN-103M and KLAN-163M wide-aperture sources of accelerated ions (Platar, Russia) according to the diagram presented in Fig. 3. Between the source of accelerated ions and a spherical workpiece, a diaphragm is placed, through which etching is carried out. The shape of the diaphragm is selected in such a way that the desired profile of aspherization is formed behind the diaphragm on the substrate surface during rotation.

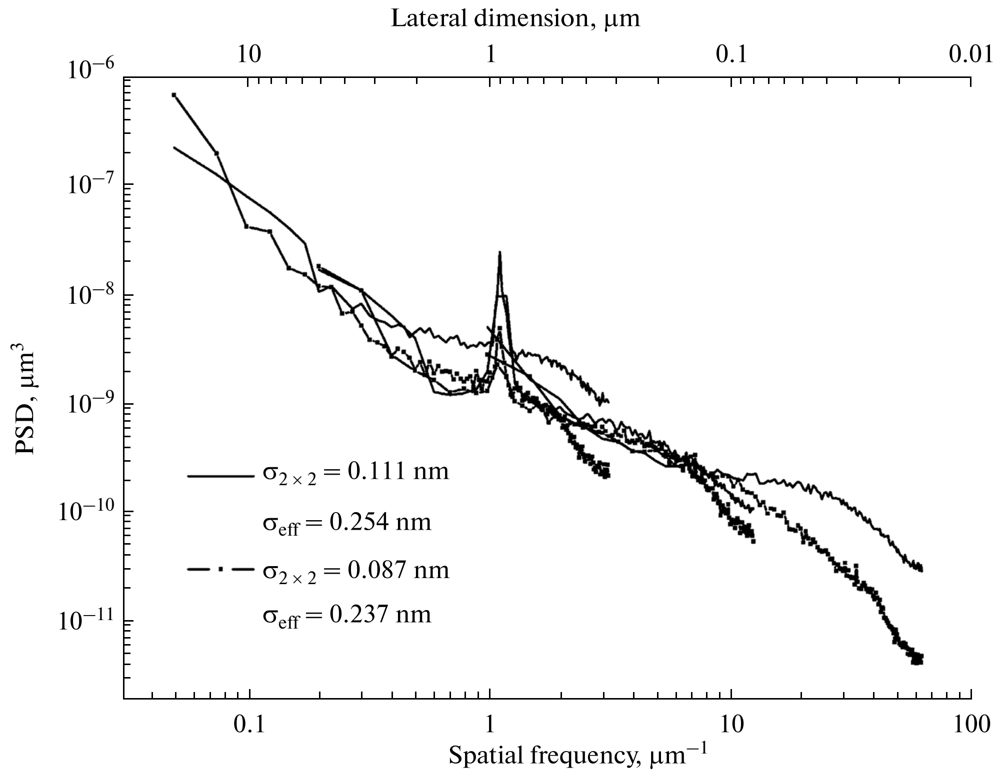

Fig. 2. PSD function of the polished fused QV quartz surface before and after etching by argon atoms ($\theta_{inc} = 90°$), plotted according to the AFM data.

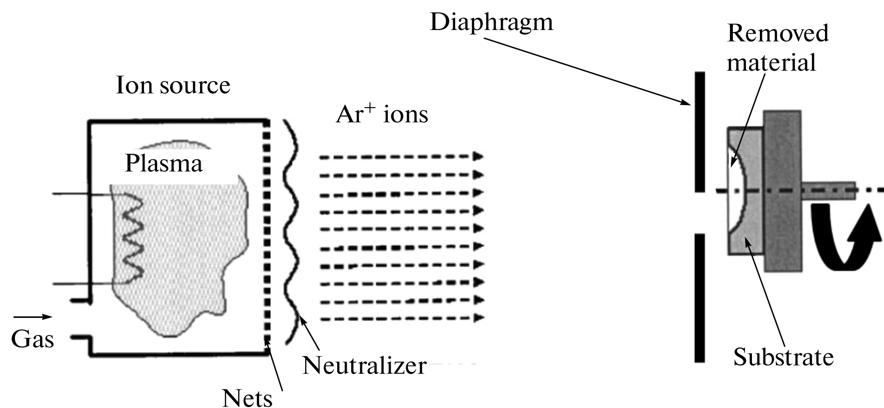

Fig. 3. Schematic diagram of the experiment on aspherization by a quasi-parallel beam of accelerated ions.

The aspherization procedure can be divided into the following steps:

(i) The distribution of the ion-beam current is determined. Figure 4 shows the ion-current distribution curves for the KLAN-103M source at a distance of 300 mm from the exit aperture (in the plane of incidence of ions on the sample surface).

(ii) The diaphragm shape is calculated considering the distribution of the ion current and the specified profile of deviation of the surface shape from a sphere.

(iii) The prepared profile is tested using flat samples, overlapped over a blank, that is, an item with the same radius of curvature as that of the actual workpiece. A part of the sample surface is covered by a mask

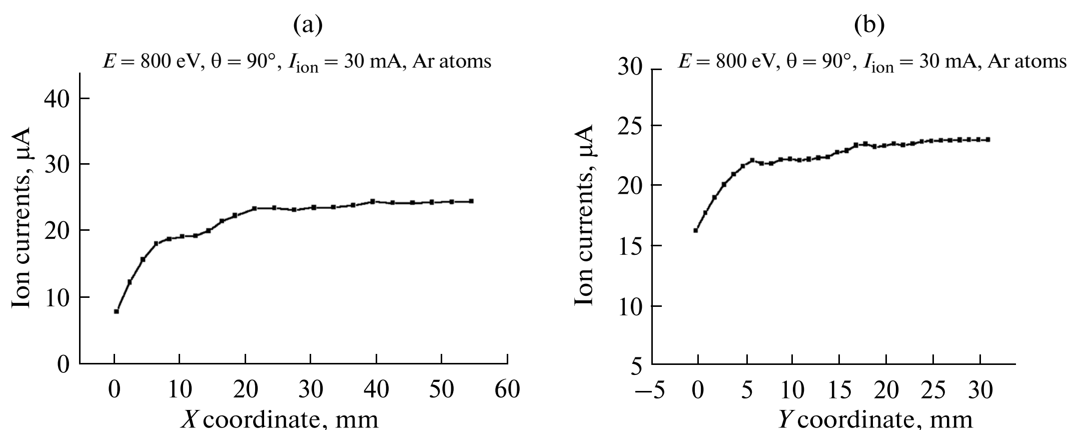

Fig. 4. Distribution of the ion current along the KLAN-103M source aperture; the exit aperture is an ellipse 90 × 60 mm in size.

extending along the radius from the rotation center to the periphery of the blank. Next, etching is performed according to the diagram shown in Fig. 3. As a result, a step is formed on the sample with distribution of the etching depth from the rotation center to the periphery. The height of the step is measured using a Talysurf CCI 2000 interference microscope.

(iv) The resulting profile is compared with the calculated values. In the case of a discrepancy between the calculated and experimental (obtained in the test sample) profiles, the shape of the mask is adjusted.

(v) If the profiles coincide, the aspherization procedure, that is, the etching of a real spherical workpiece by a quasi-parallel beam of accelerated ions through the forming diaphragm, is carried out. After formation of an aspherical surface, the surface shape of the finished sample is tested by interferometric methods.

Figure 5 demonstrates an example of the generated profile of deviation of the surface shape from a sphere: (solid line) the calculated profile, (solid square) the experimental profile prior to adjustment of the diaphragm, and (solid circle) the experimental profile after adjustment of the aperture, which was used to form the real substrate surface. It is seen that the maximum deviation from the calculated profile in the work area of the sample ($R > 10$ mm; the detail has an aperture ∅20 mm in the center) was ±13 nm; the standard deviation of the actual profile from the calculated value was no more than 4 nm.

PROCEDURE FOR SURFACE ASPHERIZATION (ASYMMETRICAL PROFILE)

In some cases, the profile of deviation of the surface shape from a sphere is not axially symmetric, such as in the Schmidt–Cassegrain-scheme mirror telescope diagram with a planoidal mirror (Fig. 6). The planoidal mirror corrects geometric wavefront aberrations and expands the angle of view of the telescope. The mirror is rotated around the optical axis, and it is obvious that corrections to the right and to the left relative to the central axis will be different.

A map of deviations from the calculated surface shape and vertical and horizontal cross sections are presented in Fig. 7. It is seen that they are substantially asymmetrical.

Such complex profiles are impossible to obtain through the forming diaphragm. Therefore, it is suggested that this problem be solved by etching with a locally focused ion beam using an ion source with a focused ion beam (Ferri Vatt, Russia).

For these purposes, a program was created simulating the trajectory and the etching time at a point for ion-beam scanning of the surface of the detail. As input data, the program receives a simulated surface being the inverted deviation of the surface shape from a sphere. The program calculates the motion trajectory of the ion beam to remove virtual bumps, which results in the desired profile of deviations from a sphere being formed on the surface.

The result of etching plates of polished fused quartz by a beam of accelerated argon ions with an energy of 800 eV, which yields an asymmetrical profile of deviation of the surface of the planoidal mirror from a plane, is presented in Fig. 8. It is seen that the curves on the left and right of the center repeat the calculated profile with good accuracy.

CONCLUSIONS

It is demonstrated in the study that the etching of polished fused quartz subjected to deep grinding and polishing by a beam of accelerated argon ions with an energy of 800 eV yields a surface roughness in the spatial-frequency range of 0.01–100 μm^{-1} on the level of 0.2–0.4 nm with material removal of more than 1 μm,

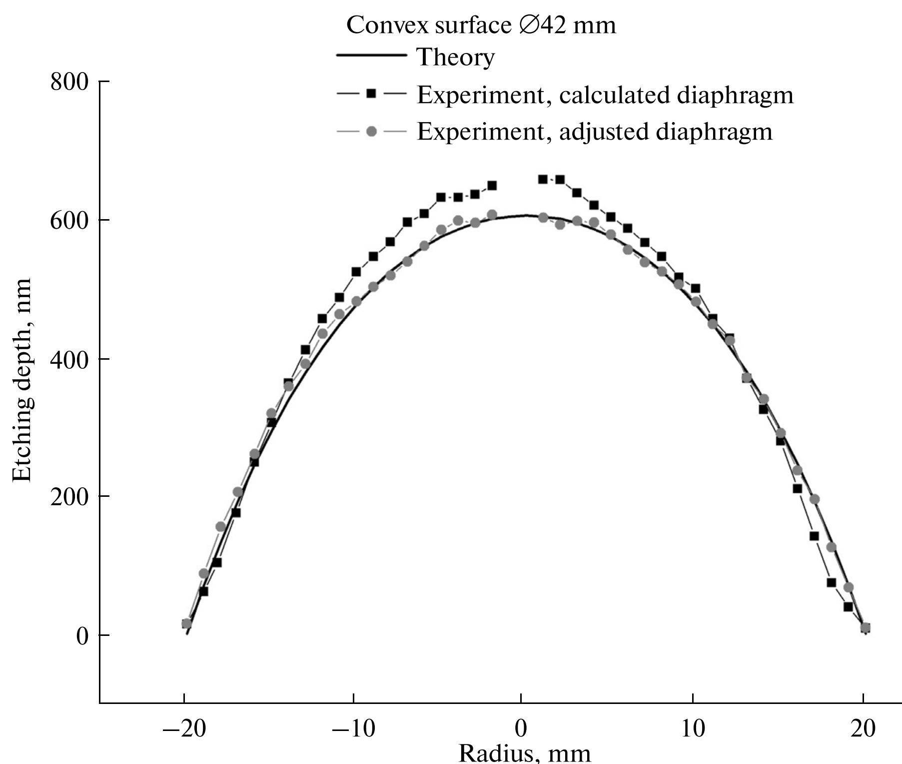

Fig. 5. Profile of deviation of the surface shape from the nearest sphere: (solid line) the calculated profile and the experimental profile (solid square) before adjustment and (solid circle) after adjustment of the aperture.

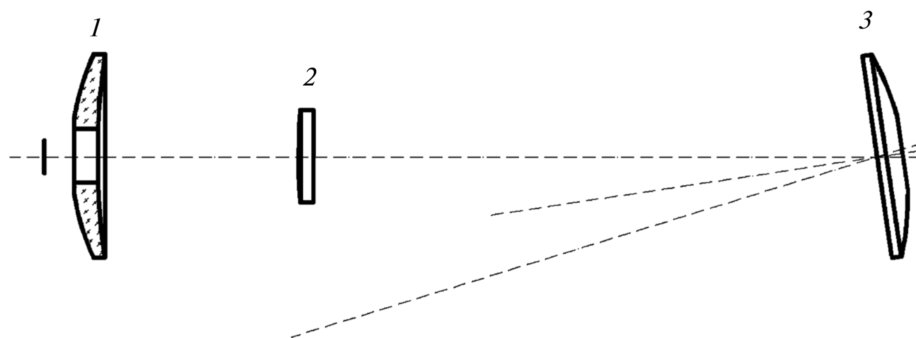

Fig. 6. Schmidt–Cassegrain telescope optical diagram with a planoidal mirror: (*1*) concave (primary) and (*2*) convex (secondary) mirrors of the lens and (*3*) planoid.

which gives the possibility of carrying out deep aspherization of the surface of optical elements with a maximum deviation from the nearest sphere of up to 100 μm.

A procedure is developed for deep surface aspherization by a quasi-parallel beam of accelerated ions through a forming diaphragm, which enables the preparation of axially symmetric aspherical surfaces with a diameter of up to 300 mm with a deviation from the calculated form of 3 nm relative to the root-mean square deviation for one cycle.

A procedure for manufacturing asymmetrical aspherical surfaces by scanning with a focused beam of accelerated ions is proposed. The procedure enables the creation of a surface with arbitrary deviation of the shape from a sphere or a plane with an accuracy on the level of nanometers relative to the standard deviation.

Thus formed optical elements may be used in super-resolution optical systems for wavelengths of

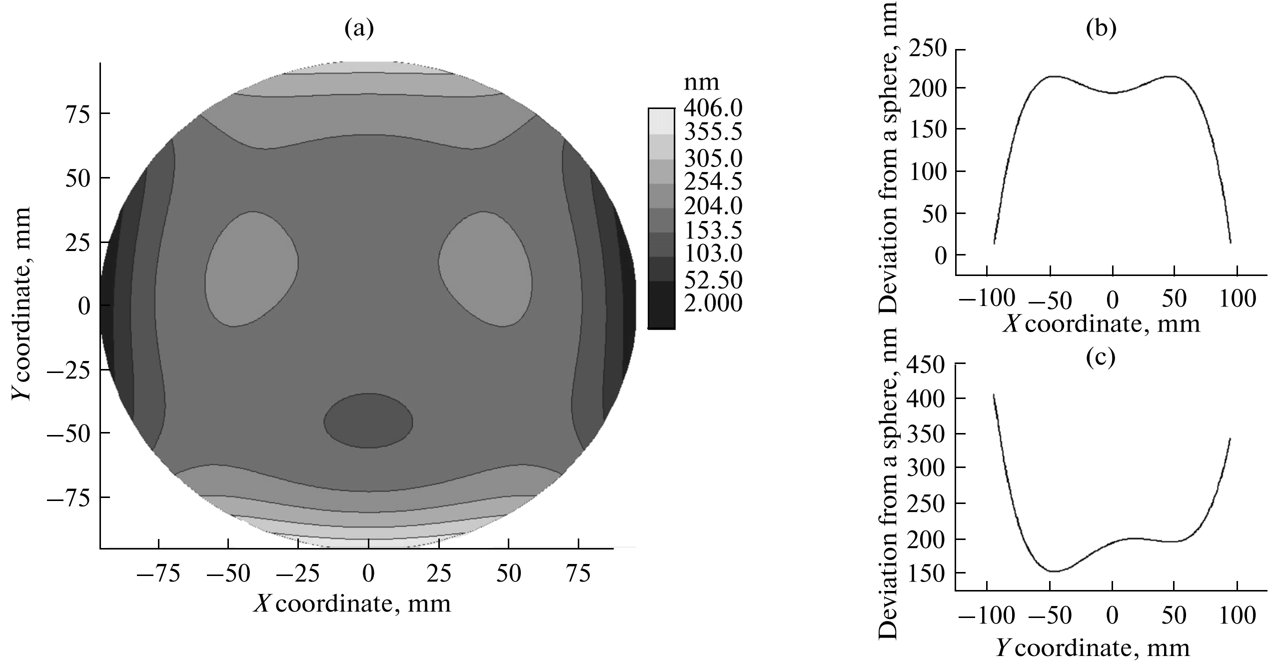

Fig. 7. Asymmetric part of the deviation of the surface shape of the planoid mirror from a plane: (a) map, (b) horizontal cross section, and (c) vertical cross section.

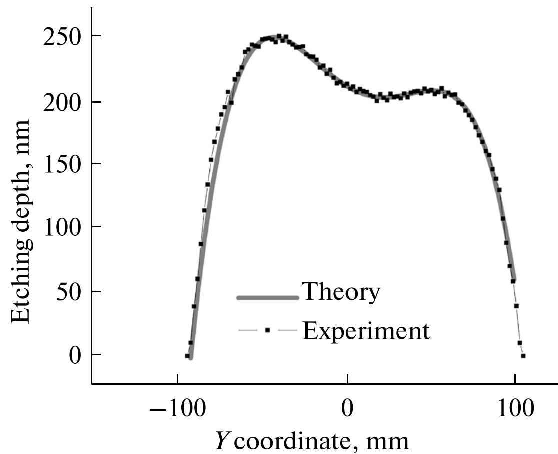

Fig. 8. Comparison of the experimental and theoretical profiles of deviation of the surface shape of the planoidal mirror from a plane.

soft X-ray and extreme ultraviolet radiation. The procedure is also applicable to the formation of aspherical elements of refractive optics of visible and ultraviolet wavelengths.

ACKNOWLEDGMENTS

The work is supported by the Russian Foundation for Basic Research, project nos. 14-02-00549, 13-02-97098, 13-02-97045, and 12-02-00659; the Ministry of Education and Science of the Russian Federation; and the Common Use Center Physics and Technologies of Micro- and Nanostructures at the Institute for Physics of Microstructures, Russian Academy of Sciences.

REFERENCES

1. E. B. Klyuenkov, A. E. Pestov, V. N. Polkovnikov, D. G. Raskin, M. N. Toropov, N. N. Salashchenko, and N. I. Chkhalo, Nanotechnol. Russ. **3**, 602 (2008).
2. M. M. Barysheva, Yu. A. Vainer, B. A. Gribkov, M. V. Zorina, A. E. Pestov, N. N. Salashchenko, R. A. Khramkov, and N. I. Chkhalo, Bull. Russ. Acad. Sci.: Phys. **76**, 163 (2012).
3. S. Yu. Zuev, E. B. Klyuenkov, A. E. Pestov, V. N. Polkovnikov, N. N. Salashchenko, L. A. Suslov, M. N. Toropov, and N. I. Chkhalo, Bull. Russ. Acad. Sci.: Phys. **75**, 53 (2011).
4. I. G. Zabrodin, B. A. Zakalov, I. A. Kas'kov, A. E. Pestov, N. N. Salashchenko, and N. I. Chkhalo, J. Surf. Invest.: X-ray, Synchrotron Neutron Tech. **7**, 913 (2013).
5. S. A. Gusev, M. N. Drozdov, E. B. Klyuenkov, A. Ya. Lopatin, V. I. Luchin, D. E. Par'ev, A. E. Pestov, N. N. Salashchenko, N. N. Tsybin, N. I. Chkhalo, and L. A. Shmaenok, J. Surf. Invest.: X-ray, Synchrotron Neutron Tech. **6**, 482 (2012).
6. I. Murakami, K. Murakami, T. Oshino, H. Kondo, et al., Proc. SPIE **6921**, 69210Q (2008).
7. I. V. Kozhevnikov, V. E. Asadchikov, A. Duparre, et al., Proc. SPIE—Int. Soc. Opt. Eng. **3739**, 348 (1999).

Translated by O. Zhukova